Int. J. Electrochem. Sci., 12 **(2017)** 7607 – 7615, doi: 10.20964/2017.08.05

International Journal of
ELECTROCHEMICAL
SCIENCE
www.electrochemsci.org

Fabrication of Immunosensor Based on Au-silica Nanocomposite for Neuron-specific Enolase Detection

Bin Wang[#], *Tao Liang*[#], *Jie Li*, *Hua Yu and Xiangyang Chu*[*]

Department of Thoracic Surgery, PLA General Hospital, No.28 Fuxing Road, Beijing, 100853, P.R. China
# These authors contribute equally
[*]E-mail: xiangyang_chu168@foxmail.com

Received: 7 April 2017 / *Accepted:* 28 May 2017 / *Published:* 12 July 2017

Neuron-specific enolase (NSE), a type of neuroendocrine molecule, is a putative serum marker for small-cell lung carcinoma. This work addressed the fabrication of a signal-enhanced, label-free, electrochemical immunosensor based on Au nanoparticle/mesoporous silica nanoparticles (Au-MSNs) for NSE determination. Because of the large number of active sites provided by the Au-SiO_2 sensor, the modified immunosensor has a significantly enhanced sensitivity. Furthermore, during quantitative NSE detection, the sensor has a desirable linear relationship with the concentration (0.1-2000 ng/mL) and a detection limit of 0.05 ng/mL.

Keywords: Label-free immunosensor; Neuron-specific enolase (NSE); Signal-enhanced; Electrochemical immunosensors; Silica

1. INTRODUCTION

Human lung cancer, including small-cell lung carcinoma and non-small-cell lung carcinoma, is the top cause of cancer death around the world [1, 2]. Fifteen to twenty percent of new lung cancer cases are attributed to the former group, and most of these cases are in an advanced disease phase when diagnosed. In this group, neuron-specific enolase (NSE), a type of neuroendocrine molecule, is used as a putative serum marker and exhibits significant diagnostic specificity and sensitivity [3]. The correlation of NSE as a cancer marker for small-cell lung carcinoma has been explored by recent studies. If the total NSE serum level is over 35 ng/mL, small-cell lung carcinoma is routinely suggested. An NSE serum assay could allow for earlier detection of cancer, and the individual management and prognosis of small-cell lung carcinoma could be improved.

With respect to lung cancer, abnormal cells grow in an uncontrolled manner in one or both lungs. Without normal functionality, the abnormal cells no longer develop and differentiate into

healthy lung tissue. Then, a tumor, i.e., a mass of tissue, is formed by the dysfunctional extra cells, and the oxygen supply from the lung to the body via blood circulation is obstructed. Lung cancer is the leading cause of cancer mortality for males and females around the world. For instance, in 2008, 31% of male and 26% of female cancer moralities were attributed to lung cancer. The risk of tumor cell metastasis and cancer recurrence still increase, even with treatment. Approximately 80% of all new cases are attributed to non-small-cell lung cancer, as proposed by the American Cancer Society. Hence, an intensive monitoring technique is necessary for non-small-cell lung cancer patients. In addition, developing proper screening approaches using NSE and other non-small-cell lung cancer marker assays is essential.

The function of an immunosensor depends on the specific reaction of antibodies with their coinciding antigens of interest, and the label's enzyme/chemical amplification [4], fluorescence [5], bioluminescence [6], radioactivity [7], electrochemical signal [8, 9], surface resonance plasmon (SPR) [10], effect on a quartz crystal microbalance (QCM) [11] or other specific activity is measured for quantification. A few immunobioluminescent assay-based approaches have been explored for NSE detection [12, 13], including two-dimensional, differential, in-gel electrophoresis [14] and mass spectrometry [15], but these approaches usually require complicated devices and complex and time-consuming specimen pretreatment. Since electrochemical immunosensors are comparatively cost-effective, rapid and highly sensitive and have low reagent consumption, they have been useful analytical devices for antigen or antibody determinations over the last few decades [16-18]. As nanotechnology has developed, electrochemical immunosensors modified using nanoparticles with distinct catalytic, thermal, electrical and optical features have garnered interest [19-21].

Ion channels are used as "smart" gates [22], and the ion current is temporarily obstructed and the current-pulse reduced upon the analyte entering the channels [23, 24]. Mesoporous silica nanoparticles (MSNs) with controllable pore diameters have been used to fabricate an electrochemical immunosensor with antibodies confined to the pore channels [25]. The peak current response indicated the obstruction of the nanopores before and after an immunological reaction. The poorly conductive silica led to weak electrical signals, which resulted in an undesirable sensitivity and poor limit of detection. Thus, this work proposes the introduction of ionic liquids, single-wall carbon nanotubes, Au nanoparticles (AuNPs) and other nanomaterials to the inner walls of MSNs to enhance the electron transportation through the channels and the detection sensitivity [26-28].

This study addressed the synthesis of MSNs and Au-MSN nanocomposites to perform a label-free NSE determination. The obtained Au-MSNs had the potential to catalyze the H_2O_2 reduction with a desirable capacity. Therefore, the highly sensitive immunosensor showed remarkable behavior and was used to detect the NSE concentration in serum specimens. The results were consistent with those obtained via the traditional clinical procedure.

2. EXPERIMENTS

2.1. Reagent

Neuron specific enolase, rabbit anti-NSE polyclonal antibody (1 mg/mL) and AP-labeled goat anti-rabbit antibody (AP-anti-IgG, 1 mg/mL) were commercially available from Beijing Biosynthesis

Biotechnology Ltd. Co. (Beijing, China). Sinopharm Chem Ltd. Co. (Shanghai, China) was the material source for N-cetyltrimethylammonium bromide (CTAB), $HAuCl_4 \cdot 4H_2O$ and tetraethoxysilane (TEOS). Graphene oxide was commercially available from XianfengNano Ltd. Co. (Nanjing, China). Sigma Aldrich (USA) was the material source for α-naphthyl phosphate (α-NP), 1-ethyl-3-(3-dimethyllaminopropyl)carbodiimide hydrochloride (EDC) (with a deacetylation degree of approximately 90%), chitosan (CS), N-hydroxysuccinimide (NHS) and bovine serum albumin (BSA). All other chemicals were of analytical grade. Ultrapure water (18 MΩ) was used for the preparation of all aqueous solutions.

2.2. Synthesis of the MSNs

The preparation of the MSNs began by dissolving 1.00 g of N-cetyltrimethylammonium bromide (CTAB, 2.74 mM) in nanopure water (480 mL). This was followed by introducing 3.50 mL of a sodium hydroxide aqueous solution (2.00 M) into the CTAB solution at a temperature of 353 K. Then, 5.00 mL of tetraethoxysilane (TEOS, 22.4 mM) was introduced dropwise into the surfactant solution with vigorous stirring, and after 120 min, a white precipitate was obtained. After filtration, the solid crude product was washed with nanopure water and methanol and dried in a high vacuum to obtain the MSNs. This was followed by refluxing the MSNs (1.50 g) in a mixture of methanol (150 mL) and HCl (37.2%, 1.50 mL) for 6 h to remove the surfactant template (CTAB). After filtration and washing using nanopure water and methanol, the terminal product, surfactant-free MSNs, was then heated to 333 K in a high vacuum to remove the residual solvent from the mesopores. After 20 h of refluxing 1.00 g of the MSNs in anhydrous toluene (80.0 mL) with 3-aminopropyltrimethoxysilane (5.67 mmol, 1.00 mL), the 3-aminopropyl-functionalized MSNs (AP-MSNs) were finally obtained.

2.3. Preparation of Au-MSNs

The synthesis of the Au-MSNs is described below. The synthesis began with the dispersion of the $HAuCl_4$ solution (0.1 M, 0.2 mL) and the obtained MSNs (10 mg) in ultrapure water (40 mL). Subsequently, the mixed solution was stirred for 1 d using a magnetic stirrer at the ambient temperature. This was followed by the dropwise addition of a $NaBH_4$ solution (50 mM). Then, the mixture was gently stirred for 5 min, centrifuged and dried under a high vacuum to obtain the terminal, solid, fresh product.

2.4. Characterizations

XRD patterns were obtained on a Bruker D8 Advance with Cu Kα radiation (λ = 0.1546 nm), and 2θ was measured in the range of 5° to 80°. Fourier transform infrared spectra (FTIR) were obtained using a Bruker Vertex 70 spectrometer.

2.5. Immunosensor fabrication

The GCE was polished with 0.3 and 0.05 μm alumina slurries to obtain a mirror-like surface and was completely rinsed with deionized water. Then, the as-prepared electrode was sonicated in acetone, nitric acid (1:1) and deionized water. After rising with deionized water again, the obtained electrode was left to dry at room temperature. This was followed by immersing the as-prepared GCE into a BSA solution (1%) for 0.5 h to obstruct the nonspecific binding sites on the surface. Subsequently, the obtained immunosensor was immersed in an incubation solution (50 μL), i.e., a mixture of the anti-NSE primary antibody (10 μL, 5 μg/mL) and NSE standard solution or serum specimen (40 μL), at 37 °C for 40 min to achieve a competitive immunoreaction. The modified immunosensor was then carefully washed with 0.01 M PBS (pH 7.4). This was followed by dropping the AP-anti-IgG/Au-MSNs (5 μL) onto the surface of the immunosensor and incubating the sensor for 40 min at 37 °C. After rinsing with 0.01 M PBS (pH 7.4), the immunosensor was used for electrochemical measurements in a DEA solution (pH 9.5) containing KCl (100 mM), $MgCl_2$ (1 mM) and diethanolamine (0.1 mM) with α-NP (1.2 mg/mL). The sensors used in this work are defined by two abbreviations, AP-anti-IgG/Au-MSNs/anti-NSE/NSE/GCE (AU-MSNs inclusive sensor) and AP-anti-IgG/anti-NSE/NSE/GCE (Au-MSNs exclusive sensor). The differential pulse voltammetric (DPV) measurements were conducted in a potential range from 0 to 0.5 V with a pulse amplitude of 50 mV.

3. RESULTS AND DISCUSSION

The Au-MSN nanocomposite constructed with Au was deposited on the MSNs. Table 1 shows that the BET surface area decreased to 408 m^2/g as the Au molecules were loaded onto the mesoporous silica surface.

Table 1. Comparison between the BET surface area for mesoporous silica and MSNPs/AuNPs nanocomposite.

Sample	S_{BET} (m^2/g)	V_p (cm^3/g)	R (Å)
MSNs	612	0.6	31
Au-MSNs	408	0.9	30

The structural features of the modified MSNP/AuNP nanocomposite were investigated using the powder XRD patterns (Fig. 1). A significant peak was observed at $2\theta = 22$ and reflects 100, which suggested the formation of an ordered mesostructure (Fig. 1A). The Au nanoparticles were characterized by the XRD profiles shown in Fig. 1B, which corresponded to the typical reflections of face-centered cubic (fcc) Au planes. The diffraction properties reflected at $2\theta = 38.18°$, 44.43°, 64.52°, and 77.46° correspond to the (111), (200), (220), and (311) planes, respectively. The XRD pattern suggests the formation of crystalline AuNPs with a fcc structure. The broadening of the XRD peaks clearly indicated that the samples were nanocrystalline in nature [29].

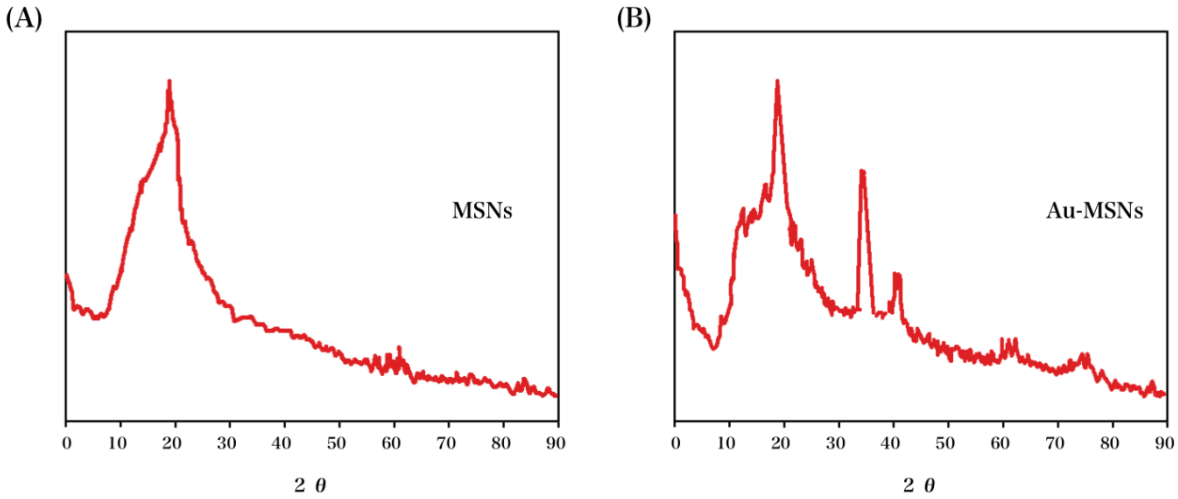

Figure 1. (A) XRD of the MSNs and (B) XRD of the Au-MSN nanocomposite.

The deposition of the Au molecules on the silica NPs was verified by the FTIR spectra of the MSNs and the Au-MSN nanocomposite (Fig. 2). The wide, broad peaks at 3269.33 and 1081.84 cm^{-1} are attributed to the NH bond and Si–O–Si bond, respectively. In addition, the 975.05 cm^{-1} peak corresponds to the Si–OH bond. As indicated in the latter spectrum, there is a dramatic decrease in the intensity of the Si—OH and Si–O–Si peaks, which suggests that the AuNPs exist in the silica NPs.

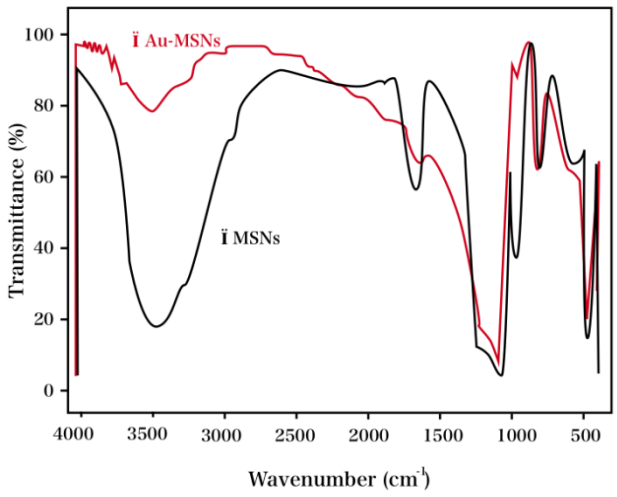

Figure 2. FTIR spectra of MSNs and Au-MSNs nanocomposite.

The optimization of the competitive immunoreactions and the specific binding of the AP-anti-IgG/Au-MSNs to the anti-NSE antibody are described below. There was a dramatic increase in the DPV peak current, and a tendency to plateau as the incubation time increased. The response was not enhanced as the incubation time increased (Fig. 3A and 3B). Therefore, the incubation time was optimized at 40 min during the incubation processes. Based on previous reports [30, 31],

electrochemical sensors should consider the preparation time in practical application development. In our case, a 60 min incubation period can be used for applications in the clinic. The anti-NSE antibody in the incubating solution was bound via competition between the target NSE and the NSE regions on the surface of the electrode during the immunoreactions. Therefore, the quantity of the anti-NSE antibody in the incubating solution played a role in the competitive immunoassay mode. The current response gradually increased during the second incubation time from 10 to 40 min and reached a maximum at 40 min. Anti-NSE antibody solutions with varied concentrations were used for the incubation of the NSE/GCEs to optimize the concentration of the anti-NSE antibody. As the concentration of the anti-NSE antibody increased, the peak current increased until 5 μg/mL, where it remained stable (Fig. 3C). This suggested a good agreement of the anti-NSE antibody and all the available recognition sites of the immobilized NSE. Hence, the anti-NSE antibody concentration of 5 μg/mL was used for the initial incubation step.

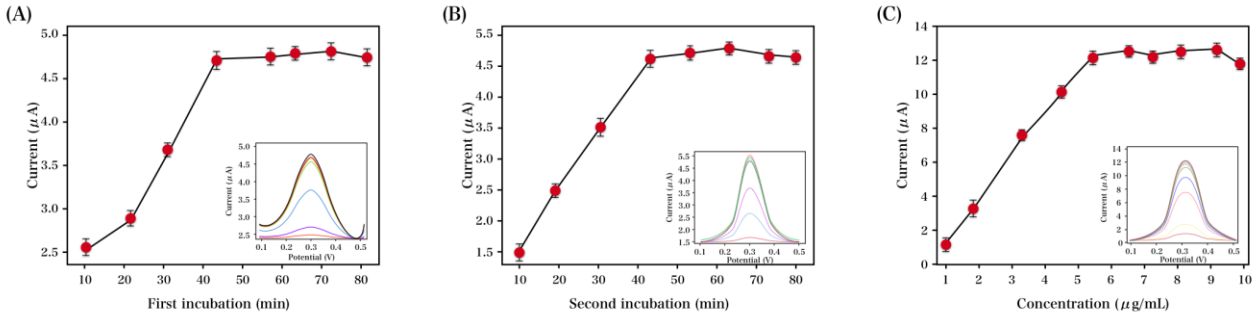

Figure 3. Effect of the peak current on the incubation time of (A) the initial incubation step and (B) the second incubation step with NSE (100 ng/mL); (C) incubation concentration of the anti-NSE as one parameter changes and the others are at their optimal conditions. The error bars represent the standard deviations calculated from three different assays.

Furthermore, the pH value of the substrate solution played a vital role in the enzyme-catalyzed reaction. A study was conducted with pH values ranging from 7.0 to 11, and the maximal response was obtained at pH 9.5 (Fig. 4A), which was the optimized value because of the highest AP activity. The electrochemical analysis performance was affected by the α-NP concentration. As the α-NP concentration increased from 0.5 to 1.6 mg/mL, the DPV peak current of the immunosensor in diethanolamine (DEA) increased and then remained stable, even at higher concentrations, as shown in Fig. 4B. Furthermore, the enzymatic reaction rate depended on the content of the AP-anti-IgG/Au-MSNs bound on the immunosensor. Therefore, the concentration of the α-NP was optimized at 1.2 mg/mL for the detection of AuNP-RGO amplified DPV.

AP-anti-IgG was used as the detection probe to bind the anti-NSE/NSE/GCE in the control group. In comparison to the control group, the analytical features of the electrochemical immunosensor using AP-anti-IgG/Au-MSNs as a detection probe were highlighted. The same batch of immunosensors were used to assay varying levels of NSE with varying detection probes, as shown in

Fig. 5. The immunosensor was used throughout the initial incubation step in the absence of anti-NSE during the control experiment, and a pronounced peak was not observed in the detection solution.

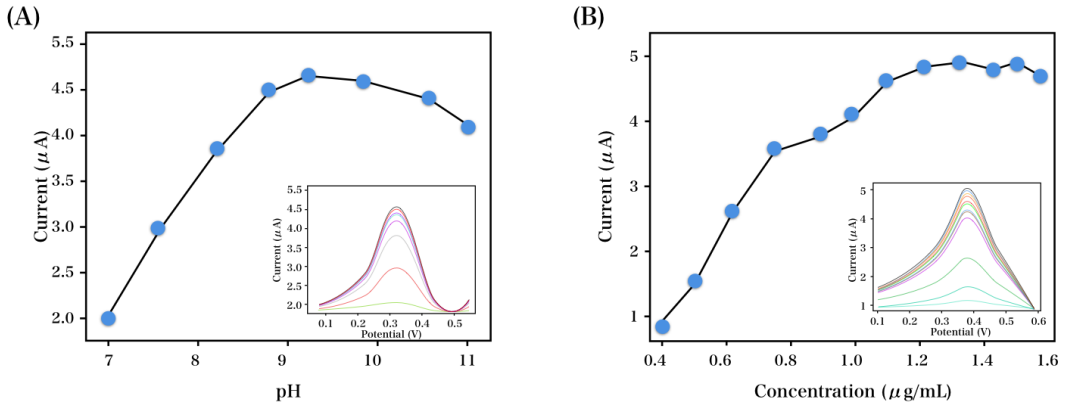

Figure 4. Effect of the peak current on the (A) pH of the detection solution and the (B) concentration of α-NP at 100 ng/mL NSE.

Nevertheless, there was an increase in the DPV signal of the blank specimen to 15.41 μA when the AP-anti-IgG/Au-MSNs was used as a detection probe, compared to 6.77 μA in the presence of AP-anti-IgG. As indicated by the aforementioned results, the AP-anti-IgG/Au-MSNs led to a significant improvement in the sensitivity of the modified immunosensor for NSE determination. The DPV peak current was reduced in proportion to the increase in the logarithm value of the NSE concentration under the optimized conditions, and a linear response was obtained from 0.1 ng/mL to 2 μg/mL with a correlation coefficient of 0.989 and a detection limit of 0.05 ng/mL. The analytical features of the obtained electrochemical immunosensor were compared to those of other candidate sensors. Other advantages of the proposed immunosensor were found and included enhanced sensitivity and a favorable capacity for detecting biomarkers at high concentrations. The excellent selectivity of the proposed immunosensor can be ascribed to the high specific surface area of the Au NPs-silica, which provide a platform for NSE and anti-NSE loading. Therefore, this technique can directly quantify the target protein over a broad concentration range in complicated clinical serum samples. The sensitivity of the AP-anti-IgG/Au-MSNs/anti-NSE/NSE/GCE was compared to that of other reported, modified electrodes, and the results are presented in Table 1. To further validate the developed immunoassay, eight rabbit tumor model samples were analyzed using the conventional immunohistochemical staining method and the proposed immunosensor. The results are shown in Table 2. The relevant faults were less than 4.22%, which indicated that the results from the two approaches agreed with each other.

Table 1. Comparison of the present AP-anti-IgG/Au-MSNs/anti-NSE/NSE/GCE with other NSE determination methods.

Electrode	Linear detection range	Detection limit	Reference
ZnCdHgSe quantum dots/polymerized ionic liquid	0.001 to 100 ng/mL	0.2 pg/mL	[32]
Poly(1,2-diaminobenzene)/SPC	0 to 50 pg/mL	—	[33]
Functional carbon nanotubes and gold nanoprobe	0.1 to 700 ng/mL	0.03 ng/mL	[34]
AP-anti-IgG/Au-MSNs/anti-NSE/NSE/GCE	0.1 to 2000 ng/mL	0.05 ng/mL	This work

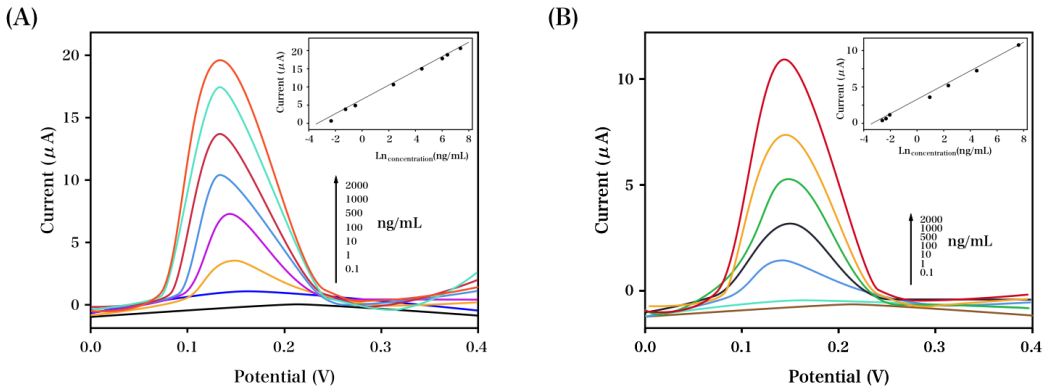

Figure 5. Typical DPV profiles of (A) AP-anti-IgG/Au-MSNs/anti-NSE/NSE/GCE and (B) AP-anti-IgG/anti-NSE/NSE /GCE obtained at 0, 0.1, 1, 10, 100, 500, 1000, 2000 ng/mL NSE.

Table 2. Determination of NSE in clinical serum samples.

Sample	Immunosensor (ng/mL)	Immunohistochemical staining (ng/mL)	RSD (%)
1	104.3	102.6	4.22
2	153.0	152.1	2.04
3	201.4	203.6	1.08
4	300.4	295.2	1.36
5	512.7	519.9	1.45

4. CONCLUSIONS

This work explored the fabrication of an electrochemical immunosensor for NSE detection at trace levels. The antibody used exhibited significant selectivity, which was shown in the detections conducted with no specimen pretreatment. The performance of the as-prepared immunosensor was remarkably improved by the modified Au-MSNs, and the sensor could perform sensitive, rapid and selective detection. Specific antigens-antibodies reactions-based immunosensors are potential candidates for ordinary analytical, physiological, biological, clinical and veterinary assays.

References

1. J. Tong, S. Yeung, A. Chan, L. Chung, S. Chau, R. Lung, C. Tong, C. Chow, E. Tin and H. Yau, *Clinical Cancer Research*, 22 (2016) 3048.
2. D. McFadden, T. Papagiannakopoulos, A. Taylor, C. Stewart, S. Carter, K. Cibulskis, A. Bhutkar, A. McKenna, A. Dooley and A. Vernon, *Cell*, 156 (2014) 1298.
3. N. Zhao, M. Wilkerson, U. Shah, X. Yin, A. Wang, M. Hayward, P. Roberts, C. Lee, A. Parsons and L. Thorne, *Lung Cancer*, 86 (2014) 255.
4. D. Cross, S. Ashton, S. Ghiorghiu, C. Eberlein, C. Nebhan, P. Spitzler, J. Orme, M. Finlay, R. Ward and M. Mellor, *Cancer Discovery*, 4 (2014) 1046.
5. Y. Zhu, J. Peng, L. Jiang and J. Zhu, *The Analyst*, 139 (2014) 649.

6. X. Yu, K. Wen, Z. Wang, X. Zhang, C. Li, S. Zhang and J. Shen, *Anal. Chem.*, 88 (2016) 3512.
7. D. Hage, *Anal. Chem.*, 71 (1999) 294.
8. N. Ronkainen and S. Okon, *Materials*, 7 (2014) 4669.
9. J. Liu, J. Wang, T. Wang, D. Li, F. Xi, J. Wang and E. Wang, *Biosensors and Bioelectronics*, 65 (2015) 281.
10. U. Eletxigerra, J. Martinez-Perdiguero, R. Barderas, J. Pingarrón, S. Campuzano and S. Merino, *Anal. Chim. Acta.*, 905 (2016) 156.
11. M. Muratsugu, F. Ohta, Y. Miya, T. Hosokawa, S. Kurosawa, N. Kamo and H. Ikeda, *Anal. Chem.*, 65 (1993) 2933.
12. R. Wevers, A. Jacobs and O. Hommes, *Clinica Chimica Acta*, 135 (1983) 159.
13. J. Viallard, M. Murthy and B. Dastugue, *Neurochemical Research*, 10 (1985) 1555.
14. L. Nejdl, H. Nguyen, L. Richtera, S. Krizkova, R. Guran, M. Masarik, D. Hynek, Z. Heger, K. Lundberg and K. Erikson, *Electrophoresis*, 36 (2015) 1894.
15. Y. Li, C. Zhou, X. Yan, J. Zhang and J. Xu, *Journal of Separation Science*, 39 (2016) 1804.
16. J. Das, . Aziz and H. Yang, *Journal of the American Chemical Society*, 128 (2006) 16022.
17. X. Liu, H. Wu, Y. Zheng, Z. Wu, J. Jiang, G. Shen and R. Yu, *Electroanalysis*, 22 (2010) 244.
18. J. Lin and H. Ju, *Biosensors and Bioelectronics*, 20 (2005) 1461.
19. M. Tu, H. Chen, Y. Wang, S. Moochhala, P. Alagappan and B. Liedberg, *Anal. Chim. Acta.*, 853 (2015) 228.
20. P. Vabbina, A. Kaushik, N. Pokhrel, S. Bhansali and N. Pala, *Biosensors and Bioelectronics*, 63 (2015) 124.
21. X. Wang, C. Chu, L. Shen, W. Deng, M. Yan, S. Ge, J. Yu and X. Song, *Sensors and Actuators B: Chemical*, 206 (2015) 30.
22. A. Escosura-Muñiz and A. Merkoçi, *Electrochemistry Communications*, 12 (2010) 859.
23. H. Bayley and P. Cremer, *Nature*, 413 (2001) 226.
24. C. Martin and Z. Siwy, *Nature Materials*, 3 (2004) 284.
25. J. Lin, Z. Wei and C. Mao, *Biosensors and Bioelectronics*, 29 (2011) 40.
26. J. Lin, Z. Wei and P. Chu, *Analytical Biochemistry*, 421 (2012) 97.
27. J. Lin, Z. Wei, H. Zhang and M. Shao, *Biosensors and Bioelectronics*, 41 (2013) 342.
28. J. Lin, H. Zhang and M. Shao, *Acta Chim Sin*, 72 (2014) 241.
29. D. Fouad, W. El-Said, M. Ali and M. El-Gahami, *Plasmonics*, (2016) 1.
30. F. Yan, Y. Zhang, S. Zhang, J. Zhao, S. Liu, L. He, X. Feng, H. Zhang and Z. Zhang, *Microchim. Acta.*, 182 (2015) 855.
31. Y. Dou, Z. Jiang, W. Deng, J. Su, S. Chen, H. Song, A. Aldalbahi, X. Zuo, S. Song and J. Shi, *Journal of Electroanalytical Chemistry*, 781 (2016) 339.
32. X. Yu, Y. Wang, X. Chen, K. Wu, D. Chen, M. Ma, Z. Huang, W. Wu and C. Li, *Anal. Chem.*, 87 (2015) 4237.
33. A. Barton, F. Davis and S. Higson, *Anal. Chem.*, 80 (2008) 9411.
34. T. Yu, W. Cheng, Q. Li, C. Luo, L. Yan, D. Zhang, Y. Yin, S. Ding and H. Ju, *Talanta*, 93 (2012) 433.